Phase-Noise-Tolerant Two-Stage Carrier Recovery Concept for Higher Order QAM Formats

Timo Pfau, *Member, IEEE*, and Reinhold Noé, *Member, IEEE*

***Abstract*—In this paper, a phase-noise-tolerant two-stage carrier recovery concept for arbitrary quadrature amplitude modulation (QAM) constellations is presented. Possible implementations are evaluated in simulations of square 16-QAM, 64-QAM, and 256-QAM transmission systems, considering fourth-power and decision-directed carrier recovery for the first stage. The second stage uses QAM feedforward carrier recovery. It is shown that the two-stage concept achieves the same phase noise tolerance as the original QAM feedforward carrier recovery concept, but reduces the required hardware effort by factors of 1.5–3 depending on the order of the QAM constellation.**

***Index Terms*—Optical fiber communication, phase estimation, phase noise, phase-shift keying (PSK), quadrature amplitude modulation (QAM).**

I. Introduction

THE NEED to increase the channel data rate in fiber optic networks without increasing the signal bandwidth drives the development toward more spectrally efficient modulation formats. Optical coherent communication systems have, therefore, been subject of intense research activities, as they have the ability to access the full information of the optical field in the electrical domain and allow to receive complex modulation formats like M-array phase-shift keying (M-PSK) or M-quadrature amplitude modulation (QAM) [1]. Today's coherent receivers rely on digital signal processing to compensate for distortions like chromatic dispersion (CD) and polarization-mode dispersion (PMD) [2], [3], nonzero intermediate frequency (IF), and phase noise [4]. For quadrature PSK (QPSK) or general *M*-PSK schemes, a multitude of carrier recovery algorithms exist that provide a high phase noise tolerance [4], [5]. However, these algorithms fail when applied to most higher order QAM constellations, because these do not have equidistant phases. Additionally, it has been shown that decision-directed carrier recovery is also not an option for higher order QAM constellations due to the inevitable feedback delay in practical systems [6].

In this paper, we review a feedforward carrier recovery algorithm for arbitrary QAM constellations that promises a phase noise tolerance sufficient to realize coherent higher order QAM receivers with DFB lasers [7]. In addition, we propose a novel extension of the algorithm to a two-stage carrier recovery concept that allows to significantly reduce the required hardware effort, while preserving the phase noise tolerance [8], [9].

Manuscript received August 25, 2009; revised September 15, 2009; accepted October 2, 2009. Date of publication December 15, 2009; date of current version October 6, 2010.

T. Pfau is with Bell Laboratories, Alcatel-Lucent, Murray Hill, NJ 07974, USA (e-mail: timo.pfau@alcatel-lucent.com).

R. Noé is with the Department of Electrical Engineering and Information Technology, Optical Communication and High-Frequency Engineering, University of Paderborn, Paderborn NRW 33098, Germany (e-mail: noe@upb.de).

Color versions of one or more of the figures in this paper are available online at http://ieeexplore.ieee.org.

Digital Object Identifier 10.1109/JSTQE.2009.2034472

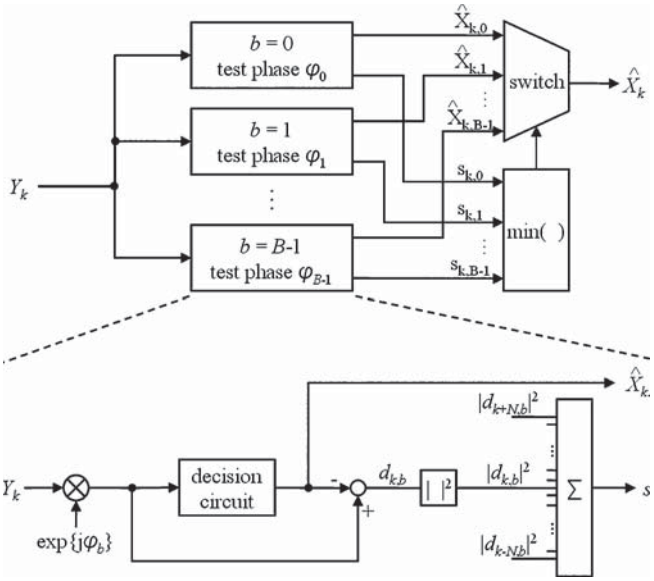

Fig. 1. QAM feedforward carrier recovery.

II. QAM Feedforward Carrier Recovery

Fig. 1 shows the block diagram of the QAM feedforward carrier recovery scheme [7]. The input signal Y_k of the coherent receiver is sampled at the symbol rate, and perfect clock recovery, equalization, and IF compensation are assumed.

The general idea of the algorithm is to simultaneously try different carrier phase angles and determine the most likely among these. Therefore, the received signal Y_k is rotated by B equidistant test carrier phase angles φ_b with

$$\varphi_b = \left(\frac{b}{B} - \frac{1}{2}\right)\gamma, \qquad b \in \{0, 1, \ldots, B-1\} \tag{1}$$

where γ is the angular size of the interval, in which the carrier phase is searched for. Hence, the difference between two neighbor test angles is $\Delta\varphi = \gamma/B$. If the input data into the carrier recovery is not preprocessed, γ has to be equal to the symmetry angle of the QAM constellation, i.e., for square QAM constellations, $\gamma = \pi/2$.

After rotation, all symbols are fed into decision circuits, and the squared distance $|d_{k,b}|^2$

$$|d_{k,b}|^2 = |Y_k e^{-j\varphi_b} - \hat{X}_{k,b}|^2, \qquad \hat{X}_{k,b} = \lfloor Y_k e^{-j\varphi_b} \rfloor_D \tag{2}$$

to the closest constellation point is calculated in the complex plane. $\lfloor . \rfloor_D$ denotes the output signal of the decision device.

In order to remove noise, the distances of $2N+1$ consecutive symbols rotated by the same test carrier phase angle φ_b are summed up for each b

$$s_{k,b} = \sum_{n=-N}^{N} |d_{k-n,b}|^2. \tag{3}$$

The optimum value of the filter halfwidth N depends on the optical SNR (OSNR) and the laser linewidth times symbol rate product.

After filtering, the optimum phase angle for symbol k is determined by searching that $b = b_{k,\min}$, which provides the minimum sum $s_{k,b}$ of distance squares. As the decoding was already executed in (2), the decoded output symbol $\hat{X}_k$ can be selected from the $\hat{X}_{k,b}$ by a switch, which is controlled by the index $b_{k,\min}$ of the minimum distance sum.

Due to the possible rotational symmetry of the QAM constellation and the resulting m-fold ambiguity of the recovered phase with $m = 2\pi/\gamma$, the receiver may not be able to uniquely assign the recovered symbol to the corresponding bits. This problem can be resolved either by using framing information [10] or by applying differential coding [11].

III. Two-Stage Carrier Recovery Concept

It has been shown in [7] that for a sensitivity penalty below 1 dB at bit error rate $(\mathrm{BER}) = 10^{-3}$, square 16-, 64-, and 256-QAM require $\geq 2^4$, $\geq 2^5$, and $\geq 2^6$ test carrier phase angles, respectively. Although a hardware-efficient implementation has been proposed to realize the algorithm, this still translates into a considerable computation effort, which could become prohibitive, especially for higher order constellations.

A possibility to further reduce the hardware effort is to preprocess the data in a first carrier recovery stage that provides a rough estimate of the carrier phase [9]. This allows to reduce the test interval γ, and hence, the number of required test carrier phase angles B for the QAM feedforward carrier recovery used in the second stage. Since only a rough estimate of the carrier phase is required after the first stage, hardware-efficient algorithms can be applied that normally fail to be sufficiently accurate in real-time higher order QAM systems, such as the fourth-power or decision-directed carrier recovery.

A. Decision-Directed Carrier Recovery

The structure of the two-stage carrier recovery using decision-directed preprocessing in the first stage is shown in Fig. 2 [12]. The input signal is derotated by the carrier phase recovered from earlier received symbols. As the second carrier recovery stage provides an accurate carrier phase estimate, no additional filter is required for the first-stage processing. The increase in complexity for the overall system due to the two-stage setup is, hence, minimal.

The critical parameter in this setup is the feedback delay Δk for the decision-directed preprocessing. The longer this delay becomes, the less accurate is the preprocessing and the larger has to be the test interval in the second stage.

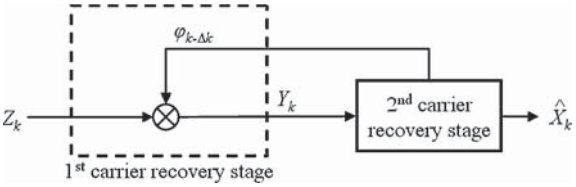

Fig. 2. Two-stage carrier recovery with decision-directed preprocessing in the first stage.

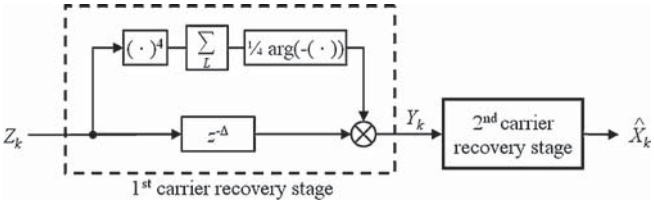

Fig. 3. Two-stage carrier recovery using fourth power phase estimation in the first carrier recovery stage.

B. Fourth-Power Carrier Recovery

To avoid any feedback in the design, the fourth-power carrier recovery algorithm can be used for the first stage, as shown in Fig. 3 [4].

In order to minimize the required computational effort, block phase estimation can be used, i.e., one carrier phase angle is calculated for a block of L consecutive symbols.

The performance of the fourth-power algorithm in combination with square QAM constellations is limited by two directly opposing properties. The fourth-power operation does not fully cancel out the modulation. Therefore, residual modulation, which can be considered as additional noise, must be mitigated by the filter. This enforces much longer filter block lengths than the ones usually required for M-PSK modulation schemes. But the longer the block length, the lower becomes the phase noise tolerance. For this reason, the fourth-power algorithm is alone suited, only to a very limited extent, for higher order QAM constellations. But a rough carrier estimation is possible with relatively low computational effort.

IV. Simulation Results

The two-stage carrier recovery is tested in MATLAB simulations for coherent square 16-, 64-, and 256-QAM transmission systems. As first carrier recovery stage, decision-directed preprocessing with a variable feedback delay of Δk symbols and fourth-power carrier recovery with variable block length L are considered. For simplicity, the second carrier recovery stage is the same for all constellations, and implemented as QAM feedforward carrier recovery with $N = 9$ and $\Delta\varphi = \pi/128$. These settings give close to optimum performance in all considered scenarios [7].

In first simulations using 100 000 symbols per data point, the accuracy of the first carrier recovery stage depending on the

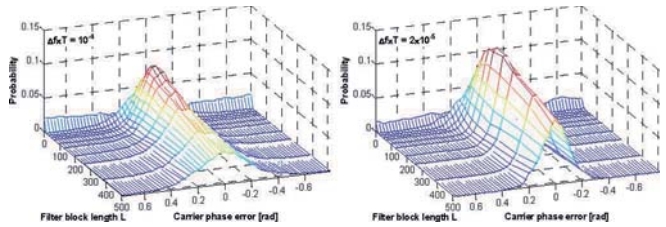

Fig. 4. Probability density functions of carrier phase error for various block lengths L of fourth-power carrier recovery, valid for square 16-QAM and $E_S/N_0 = 18$ dB.

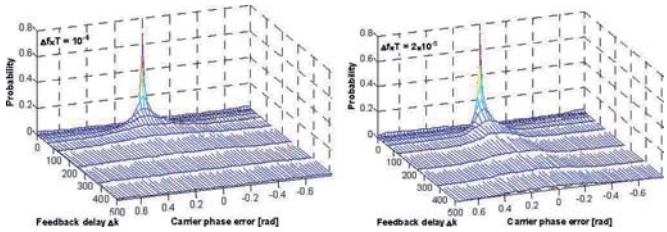

Fig. 5. Probability density functions of carrier phase error for various feedback delays Δk of decision-directed preprocessing, valid for square 16-QAM and $E_S/N_0 = 18$ dB.

applied concept and variable parameters is investigated to determine the required test interval for the second stage. The results allow to adjust the test interval in such a way that after preprocessing, the actual carrier phase is lying within this interval at a probability close to 1 (e.g., 99.999%). Then, for exemplary parameter sets, the overall receiver sensitivity is determined with 10^7 simulated symbols.

A. Square 16-QAM Carrier Recovery

Figs. 4 and 5 show the probability density functions of the carrier phase error for the two considered first estimator stages, fourth-power carrier recovery, and decision-directed preprocessing, for different feedback delays Δk and different block lengths L, respectively. Two different linewidth times symbol rate products were considered in the simulations ($\Delta f \times T \in \{10^{-4}, 2 \times 10^{-5}\}$). The normalized signal to noise ratio $E_S/N_0 = 18$ dB is selected to generate a BER close to the forward error correction (FEC) limit.

For better comparison, Fig. 6 additionally shows the carrier phase error variance as a function of the block length L of fourth-power carrier recovery and feedback delay Δk of decision-directed preprocessing, respectively.

The optimum block length for the fourth-power estimator depends on the linewidth times symbol rate product and is $L = 64$ for $\Delta f \times T = 10^{-4}$ and $L = 128$ for $\Delta f \times T = 2 \times 10^{-5}$, respectively. It allows to reduce the test interval of the second-stage estimator roughly by a factor of 2 to $[-\pi/8, \pi/8]$, as the probability that the actual carrier phase is outside this interval is negligible.

For small feedback delays, the decision-directed preprocessing achieves a very high accuracy and could work even without a second carrier recovery stage. But the estimator efficiency reduces rapidly with increasing feedback delay, and for $\Delta k > 30$ ($\Delta f \times T = 10^{-4}$) and $\Delta k > 60$ ($\Delta f \times T = 2 \times 10^{-5}$), the accuracy of the fourth-power algorithm outperforms decision-directed preprocessing. As feedback delays below these values are almost impossible to achieve in practical systems, decision-directed preprocessing is only suitable to a very limited extent for the first carrier recovery stage in combination with 16-QAM.

For comparison, Fig. 7 shows the carrier phase error distribution using QAM feedforward carrier recovery. It can be seen that the accuracy is significantly improved compared to fourth-power or decision-directed carrier recovery with realistic feedback delay. The carrier phase error variances are reduced by a factor of 10 compared to fourth-power carrier recovery with optimum block length. Hence, the second carrier recovery stage is inevitable if a high phase noise tolerance is required.

B. Square 64-QAM Carrier Recovery

For the investigation of square 64-QAM, linewidth times symbol rate products $\Delta f \times T \in \{2 \times 10^{-5}, 5 \times 10^{-6}\}$ were considered in the simulations. The normalized SNR $E_S/N_0 = 24$ dB generates a BER close to the FEC limit. Figs. 8 and 9 show the probability density functions of the carrier phase error that were achieved with the two different first estimator stages. Fig. 10 depicts corresponding carrier phase error variances.

The optimum block lengths for the fourth-power estimator are $L \approx 224$ and $L \approx 384$ for $\Delta f \times T = 2 \times 10^{-5}$ and $\Delta f \times T = 5 \times 10^{-6}$, respectively. In both cases, the performance is roughly constant for block lengths within ± 128 symbols of the optimum. The lower linewidth inherently required for a 64-QAM system compared to 16-QAM allows to use longer block lengths, which improves accuracy. The potential reduction of the test interval for the second-stage estimator is increased to a factor of 3 for $\Delta f \times T = 5 \times 10^{-6}$.

For the same reason, the estimator efficiency for decision-directed carrier recovery improved and outperforms the fourth-power algorithm as long as the feedback delay is $\Delta k < 90$ symbols for $\Delta f \times T = 2 \times 10^{-5}$ and $\Delta k < 140$ for $\Delta f \times T = 5 \times 10^{-6}$, respectively.

Fig. 11 serves as a reference and shows the carrier phase error distribution using QAM feedforward carrier recovery. Although the accuracy of the fourth-power algorithm and decision-directed carrier recovery improved for 64-QAM, the QAM feedforward algorithm still has a significantly higher accuracy. Its carrier phase error variance is more than a decade below the minimum variance of fourth-power carrier recovery.

C. Square 256-QAM Carrier Recovery

Figs. 12 and 13 show the probability density functions of the carrier phase error of the two considered first carrier recovery stages for square 256-QAM, $\Delta f \times T \in \{5 \times 10^{-6}, 10^{-6}\}$ and $E_S/N_0 = 30$ dB. The corresponding carrier phase error variances are depicted in Fig. 14.

The results continue the trend seen from 16-QAM to 64-QAM. The optimum block length for the fourth-power carrier recovery further increases for decreasing linewidth times symbol rate products and is $L \approx 448$ for $\Delta f \times T = 2 \times 10^{-5}$ and $L > 512$ for $\Delta f \times T = 10^{-6}$, respectively. Accordingly, the precision of the phase estimation increases, allowing a

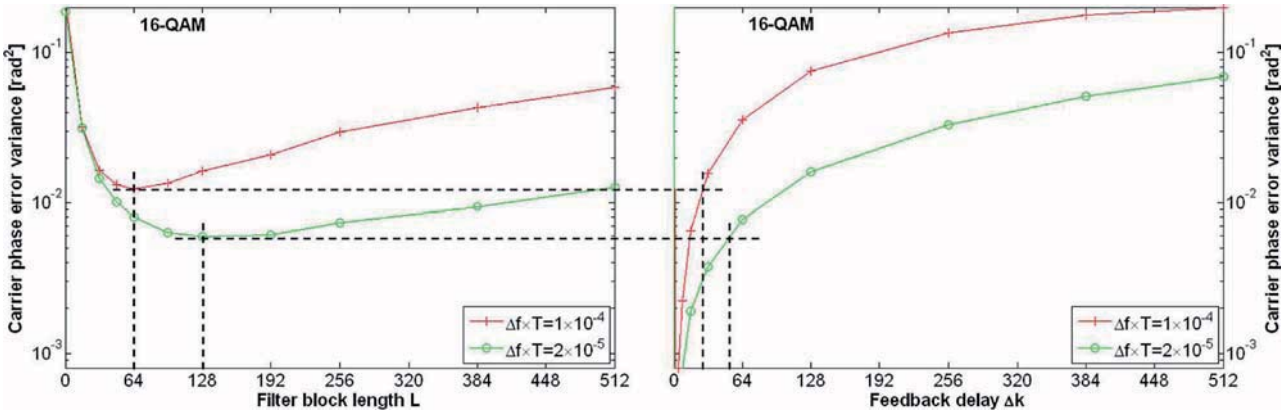

Fig. 6. Carrier phase error variance versus (left) block length L of fourth-power carrier recovery and (right) feedback delay Δk of decision-directed preprocessing, valid for square 16-QAM and $E_S/N_0 = 18$ dB.

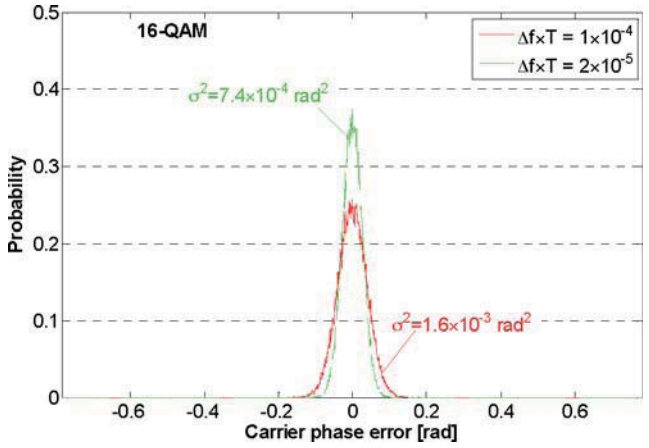

Fig. 7. Probability density function of carrier phase error for QAM feedforward carrier recovery with square 16-QAM and $E_S/N_0 = 18$ dB.

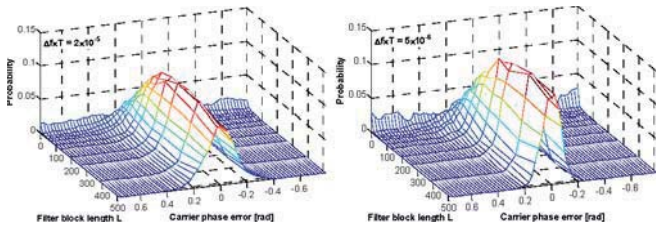

Fig. 8. Probability density functions of carrier phase error for various block lengths L of fourth-power carrier recovery, valid for square 64-QAM and $E_S/N_0 = 24$ dB.

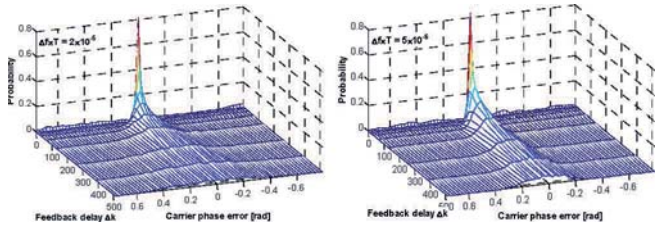

Fig. 9. Probability density functions of carrier phase error for various feedback delays Δk of decision-directed preprocessing, valid for square 64-QAM and $E_S/N_0 = 24$ dB.

reduction of the test interval for the second phase estimation stage by a factor of 3–4.

Due to the low linewidth times symbol duration products, the tolerance of the decision-directed carrier recovery against feedback delays also increased significantly. Although the performance of the fourth-power algorithm improved, it is outperformed by the decision-directed algorithm for $\Delta k < 192$ ($\Delta f \times T = 5 \times 10^{-6}$) and $\Delta k < 480$ ($\Delta f \times T = 10^{-6}$).

However, the QAM feedforward carrier recovery in the second stage (see Fig. 15) outperforms the decision-directed carrier recovery of the first stage for $\Delta k \geq 8$, achieving a carrier phase error variance of $\sigma^2 = 1.7 \times 10^{-4}$ rad^2 for $\Delta f \times T = 5 \times 10^{-6}$ and $\sigma^2 = 1.3 \times 10^{-4}$ rad^2 for $\Delta f \times T = 10^{-6}$, respectively.

D. Sensitivity of Two-Stage Carrier Recovery for Square 16-, 64-, and 256-QAM Transmission

Fig. 16 shows the achievable sensitivity for square 16-, 64-, and 256-QAM receivers using the two-stage carrier recovery concept proposed in this paper. For the 16-QAM simulations, fourth-power carrier recovery was chosen with a block length of $L = 32$ symbols and the second-stage test interval was reduced to $\gamma = \pi/3$. The 64-QAM receiver also uses fourth-power phase estimation in the first stage with $L = 192$ symbols and a second-stage test interval of $\gamma = \pi/4$. The 256-QAM receiver consists of a decision-directed carrier recovery in the first stage with feedback delay $\Delta k \geq 200$ and QAM feedforward carrier recovery in the second stage with $\gamma = \pi/6$. The reduced values of γ in the three investigated QAM constellations make it apparent that the two-stage carrier recovery concept allows for the highest reduction in required hardware for high-order QAM constellation schemes. Only $B = 22$ test carrier phase angles are required in the two-stage algorithm for 256-QAM instead of $B = 64$ in the single-stage algorithm.

As a reference, the theoretically optimum receiver sensitivity given by

$$\text{BER} = 1 - \left(1 - \frac{2}{\log_2\{M\}}\left(1 - \frac{1}{\sqrt{M}}\right)\text{Q}\left[\sqrt{\frac{3}{M-1}\frac{E_S}{N_0}}\right]\right)^2 \quad (4)$$

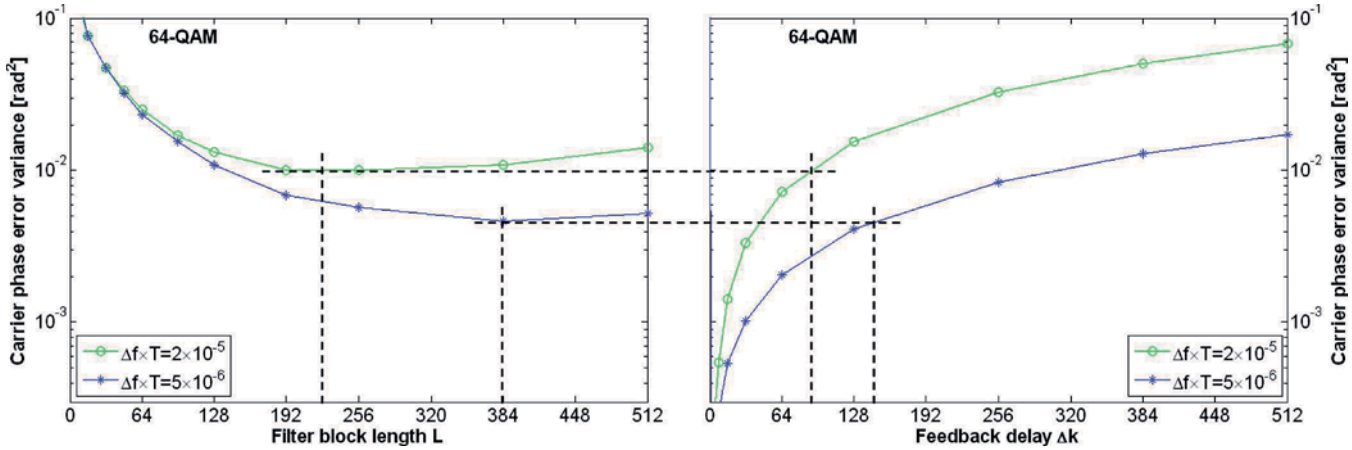

Fig. 10. Carrier phase error variance versus (left) block length L of fourth-power carrier recovery and (right) feedback delay Δk of decision-directed preprocessing, valid for square 64-QAM and $E_S/N_0 = 24$ dB.

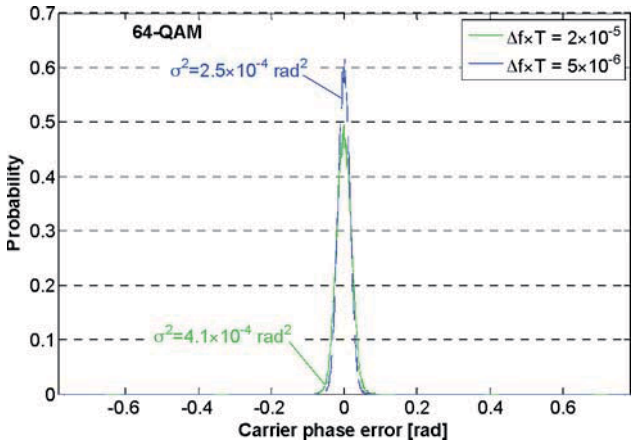

Fig. 11. Carrier phase error distribution for QAM feedforward carrier recovery with square 64-QAM and $E_S/N_0 = 24$ dB.

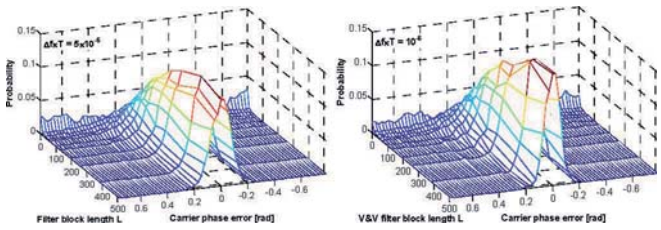

Fig. 12. Probability density functions of carrier phase error for various block lengths L of fourth power carrier recovery, valid for square 256-QAM and $E_S/N_0 = 30$ dB.

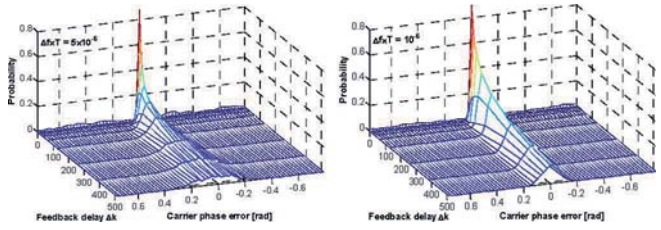

Fig. 13. Probability density functions of carrier phase error for various feedback delays Δk of decision-directed preprocessing, valid for square 256-QAM and $E_S/N_0 = 30$ dB.

where M is the number of constellation points and E_S/N_0 is the normalized measure of the energy per symbol per noise power spectral density is also plotted for the three QAM constellations [13]. The equation assumes one bit error per symbol error, which is a reasonable assumption for low BERs [14]. Note that the penalties of the simulated systems also contain a differential coding penalty.

It can be seen that the penalties for all simulated receivers are below 1 dB at BER $= 10^{-3}$ for the considered linewidth times symbol duration products and stay roughly constant down to BER $= 10^{-6}$. The only exception is 256-QAM, for which the penalty slightly increases. This can be related to $\Delta\varphi = \pi/128$, which is the same for all considered constellations. While this value leaves plenty of margin for 16-QAM and 64-QAM, it is the minimum resolution required for 256-QAM to achieve a penalty <1 dB at BER $= 10^{-3}$ [7].

The sensitivity curves clearly show that the required hardware effort for the QAM feedforward carrier recovery can be significantly reduced by applying the two-stage carrier recovery concept without sacrificing the high phase noise tolerance provided by the original concept.

V. Considerations for Practical Implementation

The large possible filter block lengths in the fourth-power carrier recovery, as well as the large feedback delay for decision-directed preprocessing, make the two-stage carrier recovery very susceptible to a residual IF. Therefore, in a practical implementation, an accurate IF compensation is required. But, it is possible to increase the IF tolerance of the algorithm by a small modification. A nonzero IF does not alter the carrier phase error variance of the first carrier recovery stage, but only causes a nonzero mean. This can be detected by monitoring the histogram of the recovered carrier angles in the second stage, and compensated by centering the test interval for the second stage at the maximum of the histogram. The size of the test interval thereby remains unchanged, which keeps the additional hardware effort for residual IF compensation very low.

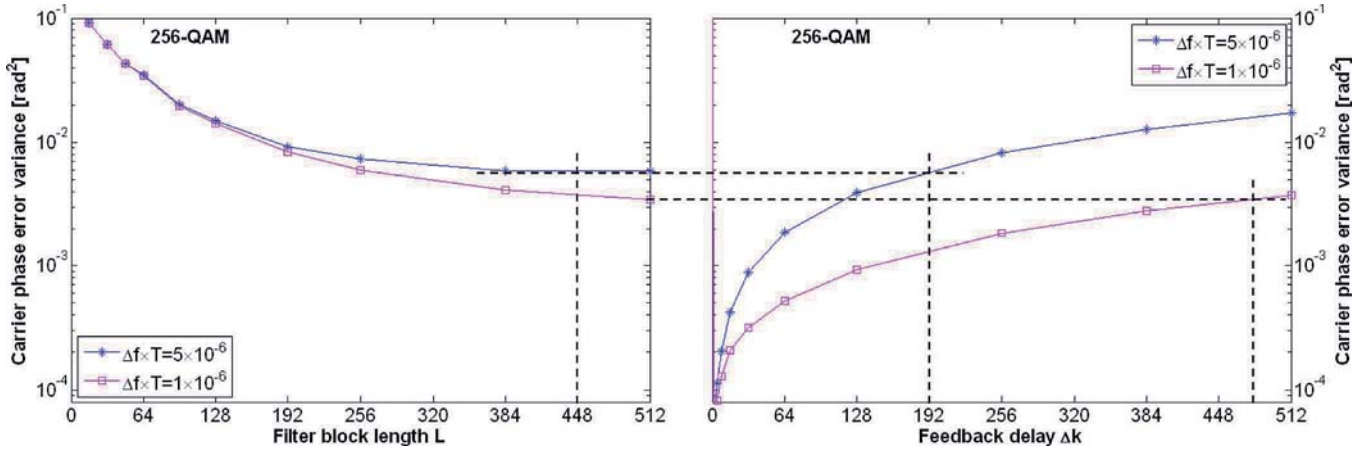

Fig. 14. Carrier phase error variance versus (left) block length L of fourth-power carrier recovery and (right) feedback delay Δk of decision-directed preprocessing, valid for square 256-QAM and $E_S/N_0 = 30$ dB.

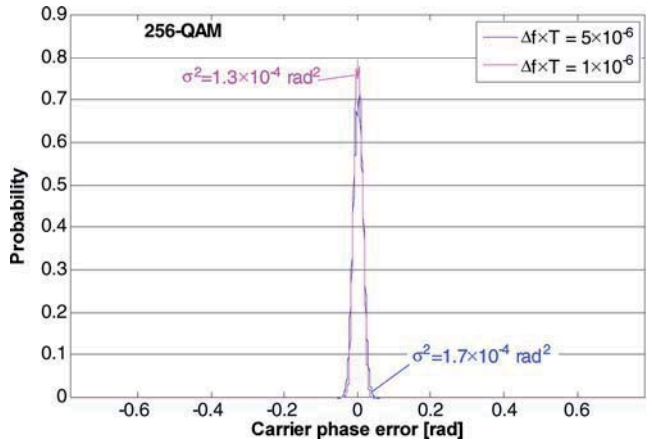

Fig. 15. Carrier phase error distribution for QAM feedforward carrier recovery with square 256-QAM and $E_S/N_0 = 30$ dB.

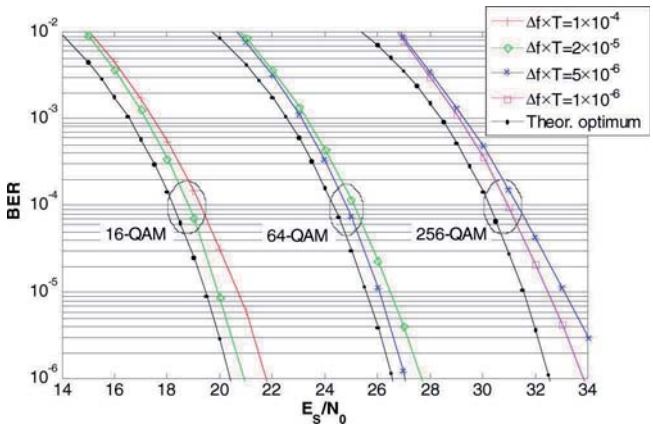

Fig. 16. Receiver sensitivity for different square QAM receivers with two-stage carrier recovery.

Another point that must be considered in a practical implementation is the startup behavior of the algorithms. The feedforward algorithms reliably recover the carrier phase as soon as their filters have been filled with samples. Using decision-directed preprocessing, this is not the case, as the initial feedback can strongly defer from the actual carrier phase. This can cause permanent errors in the decision circuits and prevent the feedback loop from locking to the correct carrier phase. Therefore, an initial training pattern might be required to guarantee locking of the decision-directed feedback loop at start up.

VI. Discussion

The proposed two-stage carrier recovery concept is highly flexible. The algorithms chosen for simulation for the first carrier recovery stage, as well as the investigated constellation diagrams, only represent examples of possible implementations. Especially for square 16-QAM, a multitude of carrier recovery algorithms have been proposed based on the fourth-power algorithm that improves its performance [15], [16]. These could further reduce the required test interval in the second carrier recovery stage, and hence, reduce the overall hardware effort of the two-stage 16-QAM carrier recovery.

In general, the proposed two-stage carrier recovery concept can be applied to any constellation diagram and can use any suitable carrier recovery concept in the first carrier recovery stage. The optimum configuration thereby varies depending on the properties of the target system.

VII. Summary

A novel two-stage carrier recovery concept has been proposed for arbitrary QAM constellations that allows to significantly reduce the hardware effort compared to the QAM feedforward carrier recovery proposed in [6], while preserving its phase noise tolerance. The concept has been verified in simulations of square 16-, 64-, and 256-QAM transmission systems, where fourth-power carrier recovery and decision-directed preprocessing have been considered as first-stage algorithms. A reduction of the required hardware by a factor of 1.5, 2, and 3 has been achieved for 16-, 64-, and 256-QAM, respectively.

References

[1] E. Ip, A. Lau, D. Barros, and J. Kahn, "Coherent detection in optical fiber systems," *Opt. Exp.*, vol. 16, no. 2, pp. 753–791, Jan. 2008.

[2] S. Savory, "Digital filters for coherent optical receivers," *Opt. Exp.*, vol. 16, no. 2, pp. 804–817, Jan. 2008.
[3] E. Ip and J. Kahn, "Digital equalization of chromatic dispersion and polarization mode dispersion," *J. Lightw. Technol.*, vol. 25, no. 8, pp. 2033–2043, Aug. 2007.
[4] R. Noé, "Phase noise tolerant synchronous QPSK/BPSK baseband-type intradyne receiver concept with feed-forward carrier recovery," *J. Lightw. Technol.*, vol. 23, no. 2, pp. 802–808, Feb. 2005.
[5] S. Hoffmann, R. Peveling, T. Pfau, O. Adamczyk, R. Eickhoff, and R. Noé, "Multiplier-free real-time phase tracking for coherent QPSK receivers," *IEEE Photon. Technol. Lett.*, vol. 21, no. 3, pp. 137–139, Feb. 2009.
[6] L. Pessoa, H. Salgado, and I. Darwazeh, "Performance evaluation of phase estimation algorithms in equalized coherent optical systems," *IEEE Photon. Technol. Lett.*, vol. 21, no. 17, pp. 1181–1183, Sep. 1, 2009.
[7] T. Pfau, S. Hoffmann, and R. Noé, "Hardware-efficient coherent digital receiver concept with feed-forward carrier recovery for *M*-QAM constellations," *J. Lightw. Technol.*, vol. 27, no. 8, pp. 989–999, Apr. 15, 2009.
[8] E. Ip and J. Kahn, "Feed-forward carrier recovery for coherent optical communications," *J. Lightw. Technol.*, vol. 25, no. 9, pp. 2675–2692, Sep. 2007.
[9] T. Pfau and R. Noé, "Algorithms for optical QAM detection," presented at the SUM 2009, Newport Beach, CA, Jul. 20–22, Paper MC3.2.
[10] E. Cacciamani and C. Wolejsza, "Phase-ambiguity resolution in a four-phase PSK communications system," *IEEE Trans. Commun. Technol.*, vol. COM-19, no. 6, pp. 1200–1210, Dec. 1971.
[11] W. Weber, "Differential encoding for multiple amplitude and phase shift keying systems," *IEEE Trans. Commun.*, vol. COM-26, no. 3, pp. 385–391, Mar. 1978.
[12] Y. Mori, C. Zhang, K. Igarashi, K. Katoh, and K. Kikuchi, "Unrepeated 200-km transmission of 40-Gbit/s 16-QAM signals using digital coherent receiver," *Opt. Exp.*, vol. 17, no. 3, pp. 1435–1441, Feb. 2009.
[13] J. G. Proakis, *Digital Communications*, 3rd ed. New York: McGraw-Hill, 1995.
[14] K. Cho and D. Yoon, "On the general BER expression of one- and two-dimensional amplitude modulations," *IEEE Trans. Commun.*, vol. 50, no. 7, pp. 1074–1080, Jul. 2002.
[15] M. Seimetz, "Laser linewidth limitations for optical systems with high-order modulation employing feed-forward digital carrier phase estimation," presented at the *OFC/NFOEC 2008*, San Diego, CA, Feb. 24–28, Paper OTuM2.
[16] H. Louchet, K. Kuzmin, and A. Richter, "Improved DSP algorithms for coherent 16-QAM transmission," presented at the ECOC 2008, Brussels, Belgium, Sep. 21–25, Paper Tu.1.E.6.

Timo Pfau (M'08) was born in Stuttgart, Germany, in 1979. He received the Dipl.-Ing. degree in electrical engineering and information technology from the University of Stuttgart, Stuttgart, in 2004, and the Dr.-Ing. degree (with highest honors) in electrical engineering from the University of Paderborn, Paderborn, Germany, in 2009.

He received a scholarship from the International Graduate School "Dynamic Intelligent Systems," University of Paderborn. Since June 2009, he has been a member of the Technical Staff at Bell Laboratories, Alcatel-Lucent, Murray Hill, NJ. His current research interests include algorithm development for DSP-based coherent optical receivers and real-time implementation of coherent optical transmission systems using advanced modulation formats.

Dr. Pfau is member of the VDE Association for Electrical, Electronic & Information Technologies. He is a Reviewer for the IEEE PHOTONICS TECHNOLOGY LETTERS, the IEEE/Optical Society of America JOURNAL OF LIGHTWAVE TECHNOLOGY, and the IEEE JOURNAL OF SELECTED TOPICS IN QUANTUM ELECTRONICS.

Reinhold Noé (M'93) was born in Darmstadt, Germany, in 1960. He received the Dipl.-Ing. and Dr.-Ing. degrees in electrical engineering from the Technische Universität München, Munich, Germany, in 1984 and 1987, respectively.

He was engaged in the development of first endless polarization control systems. For one year, he was a Postdoctoral Researcher with Bellcore, Red Bank, NJ, where he was engaged in coherent optical systems. During 1988, he was with Siemens Research Laboratories, Munich. In 1992, he implemented the first synchronous optical phase-shift keying (PSK) transmission with normal DFB lasers. Since 1992, he has been the Chair of Optical Communication and High-Frequency Engineering, University of Paderborn, Paderborn, Germany. His current research interests include high-speed endless optical polarization control and real-time synchronous QPSK transmission.